Available online at www.sciencedirect.com
SCIENCE DIRECT
Polymer 47 (2006) 1245–1258
polymer
www.elsevier.com/locate/polymer

Physical properties of poly(*n*-alkyl acrylate) copolymers. Part 2. Crystalline/non-crystalline combinations

K.A. O'Leary, D.R. Paul *

Department of Chemical Engineering and Texas Materials Institute, University of Texas at Austin, Austin, TX 78712, USA

Received 28 October 2005; received in revised form 1 December 2005; accepted 2 December 2005
Available online 10 January 2006

Abstract

The physical properties of *n*-alkyl acrylate copolymers containing one crystallizeable monomer and one non-crystallizeable or slightly crystallizeable monomer, including thermal characteristics, structure as determined by small angle X-ray scattering, and gas permeability as a function of temperature, were examined in detail and compared to the corresponding homopolymers and copolymer systems containing two crystallizeable comonomers. The current copolymers exhibit melting point depression and, for a given average side-chain length, have lower heats of fusion than the corresponding homopolymers and crystalline/crystalline copolymers. Limited SAXS experiments revealed an increase in the *d*-spacings, above and below the melting point, with side-chain length consistent with expectations. The crystallites predominantly exhibit end-to-end packing similar to other poly(*n*-alkyl acrylates) previously studied. Poly(*n*-alkyl acrylates) exhibit a 'jump' in their gas permeability at the T_m of the side-chain lengths that is mainly caused by a switch in the side-chain morphology from crystalline to amorphous upon melting. The reduced crystallinity of the crystalline/non-crystalline copolymers results in a smaller permeation jump, which in some cases were extremely broad. All jump breadths correlate with the melting endotherms for these copolymers as determined by DSC similar to that for homopolymers and crystalline/crystalline copolymers. The magnitude of the jump correlates with the heat of fusion, irrespective of the comonomer type, in all cases.

Keywords: Poly(*n*-alkyl acrylates); Gas permeation; Physical properties

1. Introduction

The first paper in this series dealt with the physical properties of *n*-alkyl acrylate copolymers consisting of two crystallizeable comonomers, referred to as crystalline/crystalline copolymers; this paper considers copolymers where there is one crystallizeable and one non-crystallizeable comonomer, referred to as crystalline/non-crystalline copolymers [1]. Poly(*n*-alkyl acrylate) homopolymers are unique in that their side-chains can crystallize independent of the backbone; however, only the side-chain carbons further than about 9–10 carbons from the backbone are able to crystallize [2–14]. Homopolymers with longer side-chain lengths (*n*) contain more carbons capable of crystallizing and, therefore, have greater melting temperatures (T_m), heats of fusion (ΔH_f), and crystalline *d*-spacings as observed by small angle X-ray scattering (SAXS) [2–4,9,14–16]. As has been extensively described in the literature, poly(*n*-alkyl acrylates) exhibit unique changes, or switch effects, in physical properties at T_m [5–8,14,16–23]. Specifically, they undergo a jump in penetrant permeability at T_m which increases in magnitude and occurs over a more narrow temperature range as the side-chain length of the homopolymer increases.

Part 1 of this series dealt with copolymers where both monomers have ten or more side-chain carbons [1]. It focused on the thermal and structural properties of the copolymers and their effects on the permeation behavior of the gases. In general, these copolymers behave similar to the homopolymers since the two types of units co-crystallize [2,7]. However, the ΔH_f, and to a lesser extent T_m, associated with this isomorphic behavior were observed to be somewhat less than the homopolymer values; this was also manifested in the gas permeation behavior. It was found that differential scanning calorimetry, DSC, provides a simple and effective method for understanding some aspects of the permeability properties and correlating them with thermal transitions.

Plots of homopolymer heats of fusion, ΔH_f, versus the number of carbon atoms in the side chain, *n*, of the homopolymer extrapolates to zero at $n=9.4$; thus, the homopolymer with $n=10$, or PA 10, is unusual in that its

* Corresponding author. Tel.: +1 512 471 5392; fax: +1 512 471 0542.
E-mail address: drp@che.utexas.edu (D.R. Paul).

0032-3861/$ - see front matter © 2006 Elsevier Ltd. All rights reserved.
doi:10.1016/j.polymer.2005.12.006

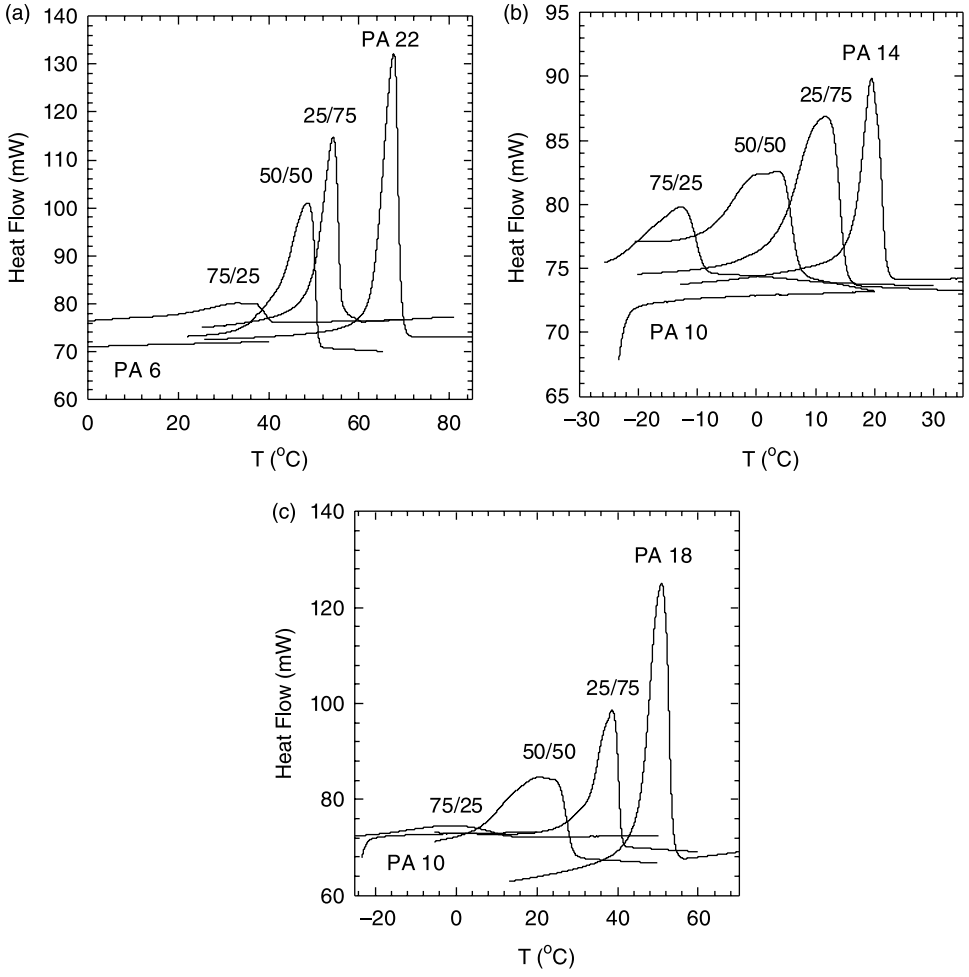

Fig. 1. DSC scans for various compositions of P(A6-*co*-A22) (a) P(A10-*co*-A14) (b) and P(A10-*co*-A18) (c) copolymers.

side-chain length is on the border of being crystallizeable. The comonomer with $n=10$ is included in both parts of this series and a heavy emphasis of this paper will be on comparing its copolymers with those containing a non-crystallizing comonomer, $n<10$. Similar to part 1, this paper will first establish the thermal and structural properties of the copolymers and then compare them with their gas permeability behavior [1].

2. Experimental

The synthesis, characterization, and analytical procedures used in this work were the same as those in part 1 [1]. Hexyl(A6) and octyl(A8) acrylates were purchased from Scientific Polymer Products, purified, and synthesized with the same methods previously described. All compositions of P(A6-*co*-A22) were solid at room temperature and solution cast while some compositions of P(A10-*co*-A14) were amorphous at room temperature and melt cast into films for permeation experiments with He, H_2, O_2, N_2, CH_4, and CO_2; however, in the intent of brevity only detailed results are shown here for O_2 and CO_2. Data for the other gases are available elsewhere [24].

3. Thermal behavior

Several prior studies have reported on the thermal properties of poly(*n*-alkyl acrylate) copolymers having one crystallizeable and one non-crystallizeable comonomer [4–7,18]. Greenburg and Alfrey reported an early study on the melting temperatures of P(A1-*co*-A18) and P(A1-*co*-A16) [4]. Jordan later reported a thorough investigation of copolymers of methyl, ethyl, butyl, and octyl acrylates with A18 [7]. Jordan described the acrylates unable to crystallize as 'spacers' because they depress the T_m and ΔH_f by interrupting the ordered long side chains of A18 without crystallizing in the lattice [7].

In main-chain copolymers, a non-crystallizeable comonomer concentration as low as 25 mol% may entirely prevent any crystallization [2]. Side-chain copolymers, with flexible amorphous backbones and proximal side-chain carbons, can crystallize when the non-crystallizeable comonomer content is as high as 90 mol% [2,7]. Non-crystallizeable comonomers affect the copolymer in several ways. First, they reduce the overall number of crystallizeable carbons in the copolymer; second, they interrupt and impede the crystallizeable side chains from forming perfect crystals;

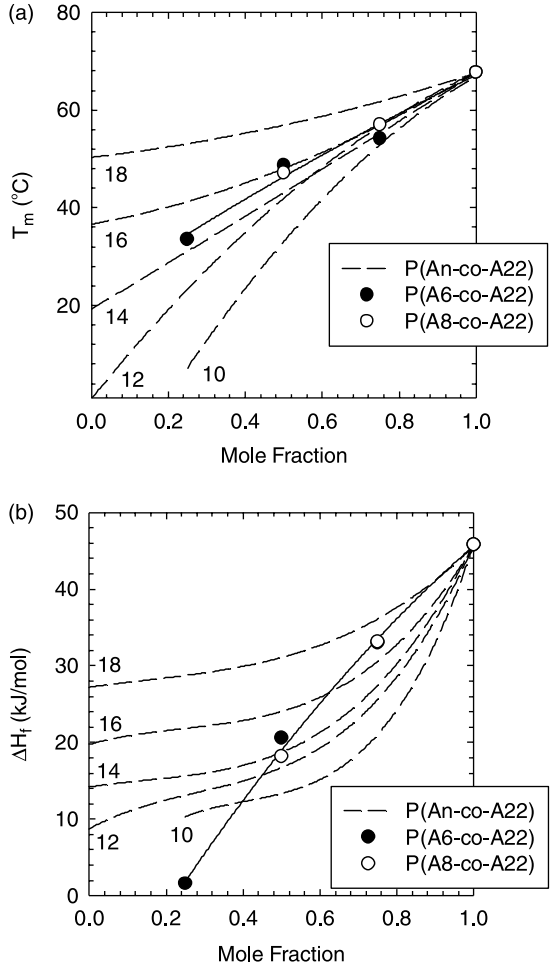

Fig. 2. Dependence of T_m (a) and ΔH_f (b) on the composition of copolymers based on A22 and other *n*-alkyl acrylate monomers. The data points shown are for copolymers containing spacers, P(A6-*co*-A22) and P(A8-*co*-A22), while the dashed lines represent copolymers containing two crystallizeable comonomers, P(A*n*-*co*-A22).

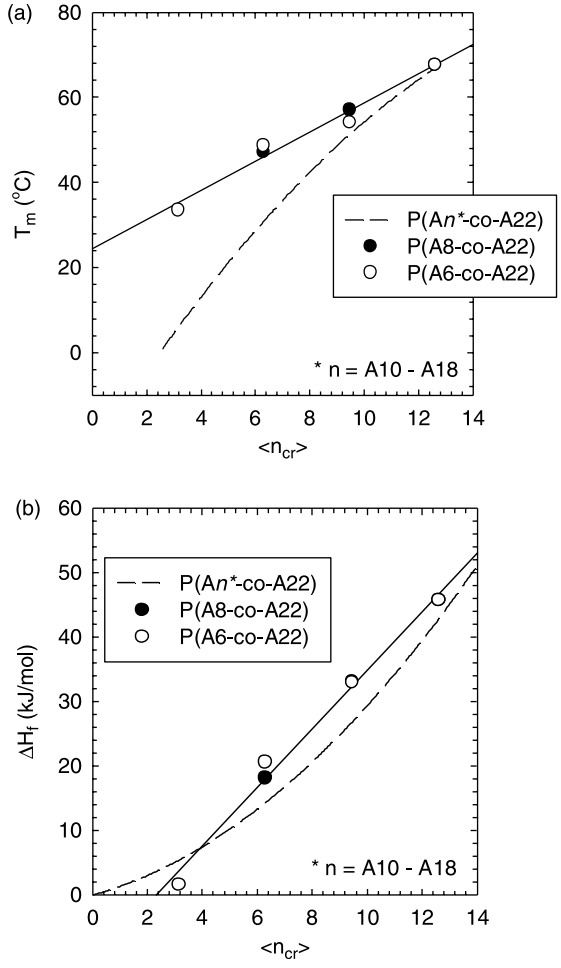

Fig. 3. Dependence of T_m (a) and ΔH_f (b) on the number of crystallizeable side-chain carbons, $\langle n_{cr} \rangle$, for materials based on monomer A22 and other *n*-alkyl acrylate monomers. The data points are for copolymers containing spacers, P(A6-*co*-A22) and P(A8-*co*-A22), while the dashed lines represent copolymers with two crystallizeable comonomers, P(A*n*-*co*-A22). The average number of crystallizeable carbons $\langle n_{cr} \rangle$, was calculated via Eq. (1).

Table 1
Melting temperature, heat of fusion, and molecular weight for poly(*n*-alkyl acrylate) copolymers

Copolymer	Monomer 1[a] (mol%)	Average side-chain length $\langle n \rangle$	T_m (°C)	ΔH_f (kJ/mol)	Copolymer $\bar{M}_W$
P(A10-*co*-A14)	75	11	–	–	215,000
	50	12	3.7	4.8	141,000
	25	13	11.9	9.5	191,000
P(A10-*co*-A18)	75	12	−1.1	7.6	185,000
	50	14	21.2	11.8	235,000
	25	16	38.5	21.3	197,000
P(A6-*co*-A22)	75	10	33.5	1.6	186,000
	50	14	48.7	20.6	210,000
	25	18	54.2	33.0	237,000
P(A8-*co*-A22)	75	11.5	–	–	255,000
	50	15	47.2	18.2	149,000
	25	18.5	57.0	33.2	187,000
P(A10-*co*-A22)	75	13	6.4	10.3	201,000
	50	16	35.5	13.3	253,000
	25	19	50.5	21.0	189,000

[a] Note that monomer 1 refers to the first monomer listed in the copolymer, i.e. for P(A10-*co*-A18), monomer 1 refers to A10.

and, third, they force the amorphous backbone to contort to accommodate the side chains crystallizing around the non-crystallizeable side-chains which hinders the conformational freedom of the backbone [2,5–7]. These effects reduce the overall crystallinity which, in turn, depress the T_m and ΔH_f of the copolymers.

DSC thermograms for the copolymer systems P(A6-*co*-A22), P(A10-*co*-A14), and P(A10-*co*-A18) are shown in Fig. 1. All data were recorded on the second heat. Just as with the crystalline/crystalline copolymers, these copolymers show a single melting peak that grows broader and smaller in area as the concentration of the shorter side-chain length comonomer increases resulting in an overall increase in smaller crystals. In the case of P(A6-*co*-A22), the A6 comonomer inhibits the crystallization of A22 units by physically separating them which causes the formation of small and more imperfect crystals. As discussed in part 1 [1], the crystal lattices of the P(A10-*co*-A14) and P(A10-*co*-A18) copolymer systems are ambiguous because A10 is technically

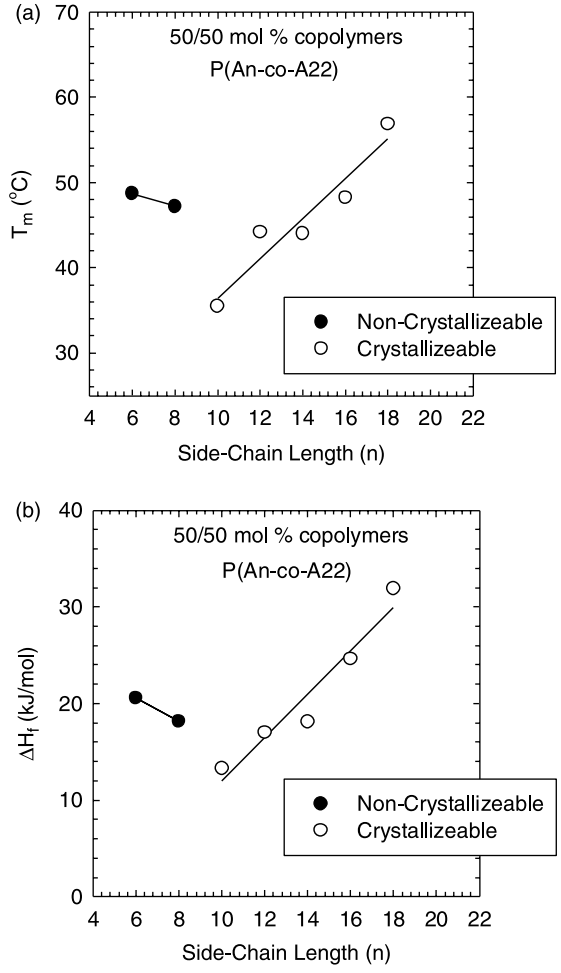

Fig. 4. Dependence of T_m (a) and ΔH_f (b) of copolymers of P(A*n*-*co*-A22) with 50:50 mol% based on the side-chain length of the comonomer with the shorter alkyl unit. The solid points are for copolymers containing spacers, P(A6-*co*-A22) and P(A8-*co*-A22), while the open points are for copolymers with two crystallizeable comonomers, P(A*n*-*co*-A22), i.e. where *n* is 10 or more.

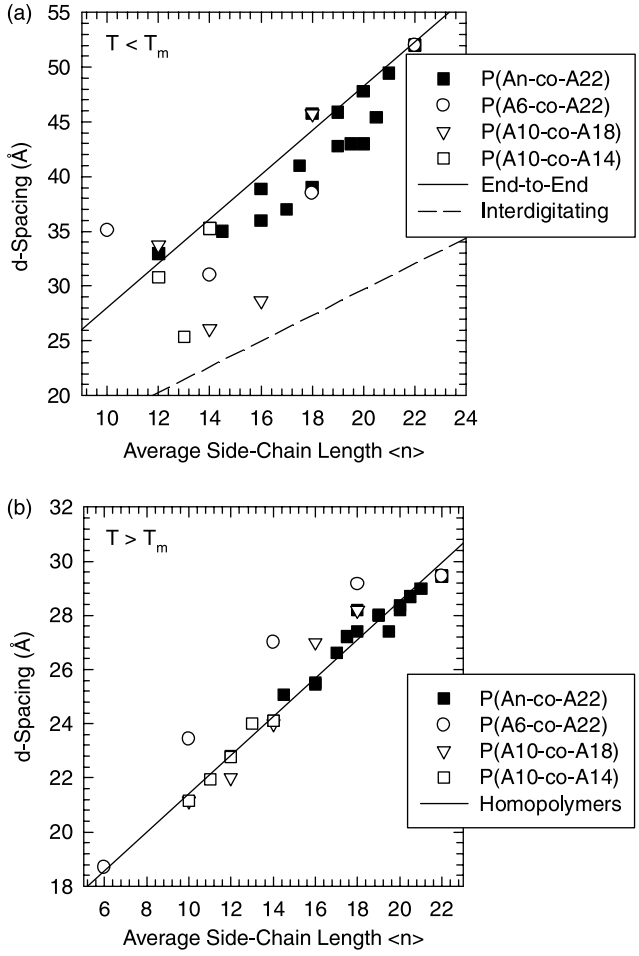

Fig. 5. Small angle X-ray *d*-spacings for homopolymers (lines) and poly(*n*-alkyl acrylate) copolymers (points) measured in the semi-crystalline (a) and amorphous (b) states. For the crystalline polymers, the upper homopolymer line reflects the *d*-spacing for end-to-end crystal packing while the lower line represents the *d*-spacings for interdigitating crystal packing as reported by Plate.

Table 2
d-Spacings for amorphous and crystalline copolymers

Copolymer	Monomer 1 (mol%)	Average side-chain length ⟨*n*⟩	Molten *d*-spacing (Å)	Crystalline *d*-spacing (Å)
P(A6-*co*-A22)	100	6	18.7	–
	75	10	23.4	33.0
	50	14	27.0	34.0
	25	18	29.2	36.5
	0	22	29.5	52.0
P(A10-*co*-A14)	100	10	21.2	–
	75	11	21.9	–
	50	12	22.8	24.6
	25	13	23.6	30.7
	0	14	24.1	35.3
P(A10-*co*-A18)	100	10	21.2	–
	75	12	22.0	28.3
	50	14	24.0	29.1
	25	16	27.0	33.6
	0	18	28.2	45.7

crystallizeable at low enough temperatures; however, the ability of this comonomer to substantially crystallize into a lattice with other comonomers is questionable. The thermograms in Fig. 1(b) and (c) for P(A10-*co*-A14) and P(A10-*co*-A18) are similar to those for P(A6-*co*-A22) in Fig. 1(a). These figures suggest that both types of copolymer systems have reduced crystallinity and crystallite size with increasing composition of the smaller comonomer.

The data points and solid lines in Fig. 2(a) and (b) represents the T_m and ΔH_f versus the mole fraction of A22 units in copolymers with A6 and A8, also see Table 1. The dashed lines represent the results for copolymers of A22 with other *n*-alkyl acrylates with *n* ranging from 10 to 18, i.e. crystalline/crystalline copolymers reported in Fig. 4(a) and (b) of part 1 [1,24]. The values of T_m and ΔH_f for P(A6-*co*-A22) and P(A8-*co*-A22) copolymers are nearly the same at a given mole fraction of A22; the trend or progression with *n* for these copolymers is clearly different than that for the series where *n* is 10 or more, i.e. where co-crystallization occurs. The T_m

curves for $n=6$ and 8 are in about the same range as seen for copolymers of A22 with *n*-alkyl acrylate monomers having $n=14$–16. On the other hand, the ΔH_f curves crosses the lines shown for the systems that co-crystallize and approaches zero at just over 20 mol% of A22. While the P(A6-*co*-A22) and P(A8-*co*-A22) copolymers show nearly identical T_m and ΔH_f trends, P(A10-*co*-A22) falls in the progression observed for crystallizeable–crystallizeable copolymers. The latter shows the largest depression in ΔH_f because of the differences in side-chain lengths between A10 and A22 entering the lattice. This indicates that when copolymerized with A22, A10 behaves like a crystallizeable polymer in terms of T_m and ΔH_f. This also appears to be the case in Fig. 3(a) and (b) from part 1 [1] for P(A10-*co*-A14) and P(A10-*co*-A18). The difference in behavior between P(A10-*co*-A22) and P(A8-*co*-A22) is the most dramatic considering A8 and A10 only differ by two side-chain carbons.

The T_m and ΔH_f values for copolymers can be plotted as a function of the average number of crystallizeable side-chain carbons $\langle n_{cr} \rangle$, as shown in Fig. 3(a) and (b). This quantity is defined as follows

$$\langle n_{cr} \rangle = (n_1 - 9.4)x_1 + (n_2 - 9.4)x_2 \quad (1)$$

where n_1 and n_2 are the number of carbon atoms in the longer and shorter side-chain lengths, respectively, and x_1 and x_2 are the mole fractions of these monomer units. When comonomer 2 has fewer than 9.4 carbon atoms in its side chain, i.e. $(n_2 - 9.4) < 0$, this term in Eq. (1) is set equal to zero, since a comonomer with fewer than 9.4 carbons cannot crystallize. This is a convenient way of comparing the T_m and ΔH_f of the different types of copolymers based on the

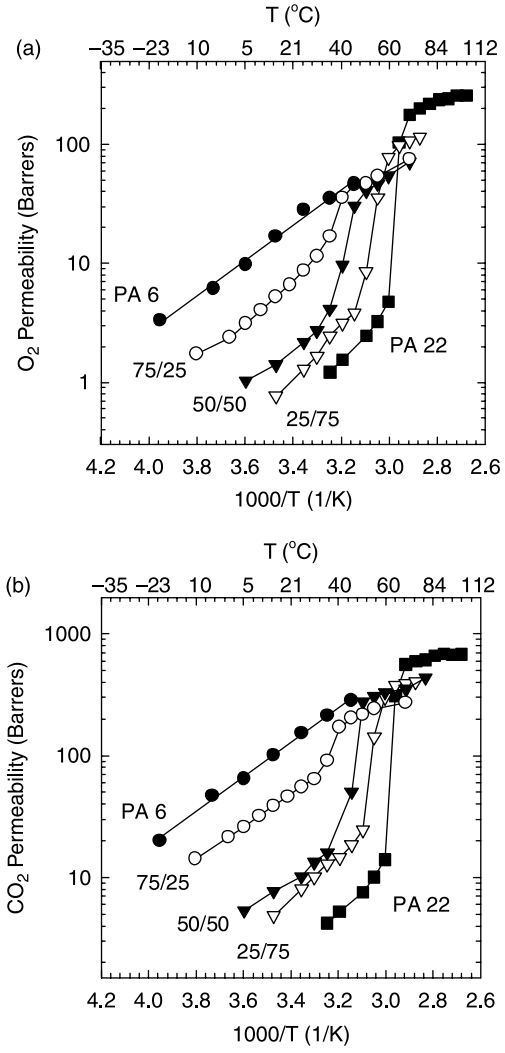

Fig. 6. Permeability of O_2 (a) and CO_2 (b) in P(A6-*co*-A22) copolymers as a function of temperature plotted on Arrhenius coordinates.

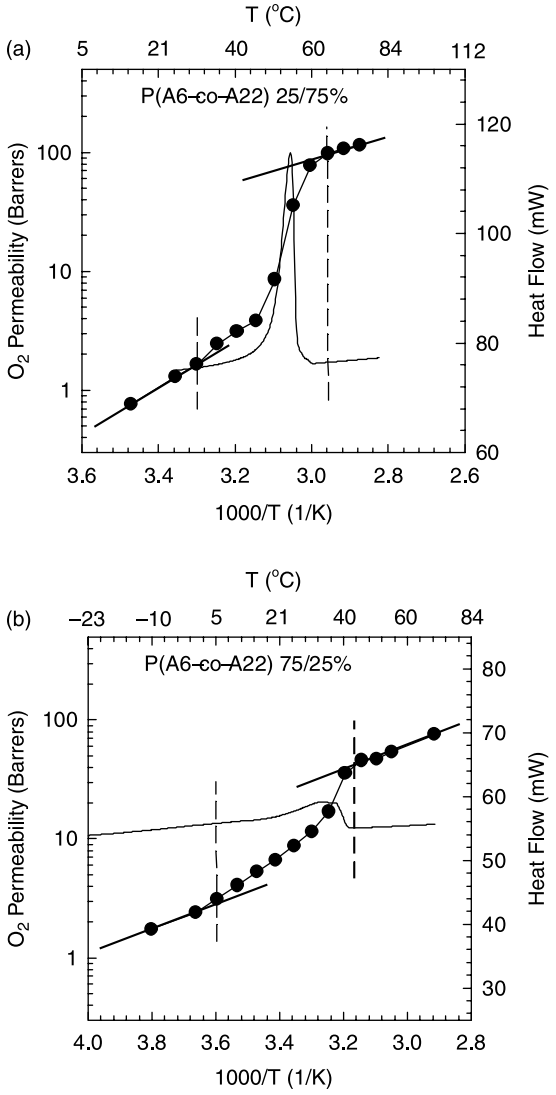

Fig. 7. Permeability of O_2 in (a) P(A6-*co*-A22) with 25:75% and (b) with 75:25% as a function of temperature on Arrhenius coordinates with DSC thermograms superimposed on the same temperature scale. The onset and end temperature of the melting peak and permeation jumps are marked with dashed lines.

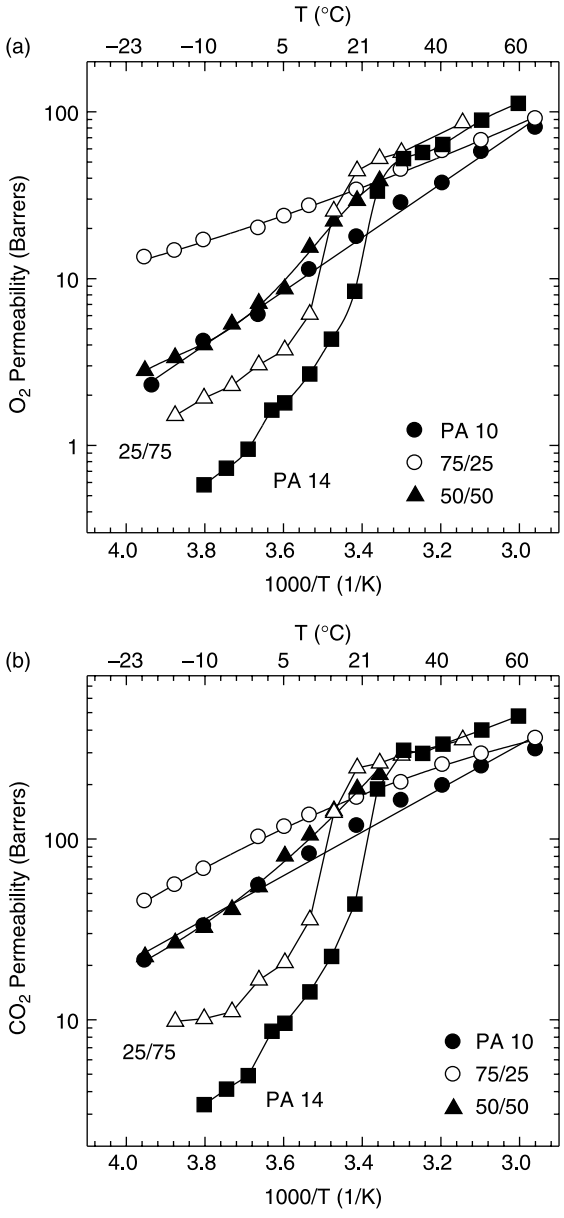

Fig. 8. Permeability of O_2 (a) and CO_2 (b) in P(A10-*co*-A14) copolymers as a function of temperature on Arrhenius coordinates.

average number of carbons participating in the crystal lattice rather than all the side-chain carbons. Although T_m and ΔH_f for all copolymer systems decrease as $\langle n_{cr}\rangle$ decreases, those for the A6 and A8 copolymer systems decrease less rapidly than the P(A*n*-*co*-A22) systems in Fig. 3(a). This is the difference between systems that co-crystallize versus systems that experience melting point depression or the 'spacer' effect in the terminology of Jordan [7]. The comonomers capable of co-crystallizing with A22 units have a greater effect on the T_m than the 'melting point depression' caused by either A6 or A8. The A6 and A8 spacers do not have as great an effect on T_m, since, they simply impede crystal formation rather than actually altering the basic nature of the crystal itself. These effects are also apparent in Fig. 3(b) where it is shown that ΔH_f of all copolymers decrease with decreasing number of crystallizing side-chain carbons; reducing the composition of A22 decreases the number of carbons capable of crystallizing. The ΔH_f of P(A6-*co*-A22) and P(A8-*co*-A22) more or less decrease linearly with $\langle n_{cr}\rangle$ and goes to zero at $\langle n_{cr}\rangle$ just over 2. Note that the side-chain carbons of A22 are the only units that can form crystals. For the copolymers of A22 with *n*-alkyl acrylates with $n=10$ to 18, ΔH_f shows a non-linear relationship that goes to zero at $\langle n_{cr}\rangle=0$. For $\langle n_{cr}\rangle$ less than 4, ΔH_f for the co-crystallizeable copolymers are lower than for those where co-crystallization does not occur. These trends reflect the physical differences between altering the nature of the crystal by co-crystallization versus restricting the ability of the copolymer to crystallize by reducing the conformational freedom of the backbone and, thereby, forcing the A22 side chains to form less perfect crystals. These trends are similar to observations reported by Jordan for the P(A8-*co*-A18) system [7].

The consequences of these differences are more clearly shown by plots of T_m and ΔH_f for 50:50 mol% copolymers of A22 versus the number of carbons in the side chain of the shorter comonomer as seen in Fig. 4. Copolymers of A22 with the non-crystallizeable comonomers A6 and A8 are represented by the solid points while those with the crystallizeable comonomers, A10, A12, A14, A16, and A18, are represented by open points. The T_m and ΔH_f curves show exactly opposite trends with *n* for the two types of systems with a minimum appearing at $n\approx 10$ for both T_m and ΔH_f.

4. Structural analysis

Two prior small angle X-ray scattering (SAXS) studies have been reported for poly(*n*-alkyl acrylate) copolymers containing one long, crystallizeable comonomer and one non-crystallizeable comonomer [2,5,6]. Although each investigated a single copolymer system, both reported similar findings involving the packing structure of the side chains. Unlike the crystallizeable/crystallizeable copolymers examined in part 1 [1], the copolymers with only one crystallizeable comonomer described here had relatively low melting temperatures which limited the number of samples that could be examined in the crystalline state by SAXS. Therefore, the SAXS results reported provide only a small glimpse into the structural behavior of these polymers adding to the initial studies by Plate and Hsieh; however, it is not thorough enough to draw any definitive conclusions or to attempt modeling their behavior as was done in part 1 of this series [1,2,5,6].

Hsieh and Morawetz studied P(A1-*co*-A16) copolymers and observed both interdigitating and end-to-end side-chain packing forms, illustrated in Fig. 9(a) and (b) of part 1 [1], as well as a strong increase in *d*-spacing values as the concentration of A1 increased, although the average side-chain length and amount of crystallinity decreased in these copolymers [1,5,6]. Plate and Shibaev reported on

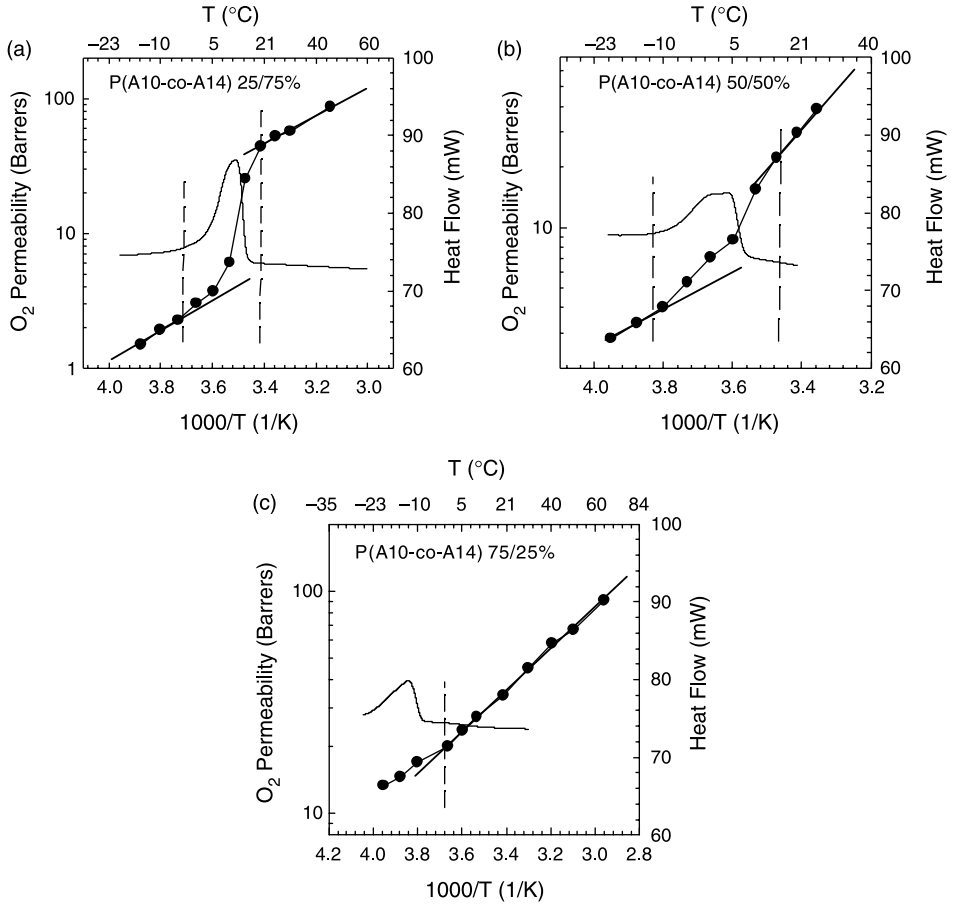

Fig. 9. Permeability of O_2 in (a) P(A10-*co*-A14) with 25:75%, (b) 50:50%, and (c) 75:25% as a function of temperature on Arrhenius coordinates with DSC thermograms superimposed on the same temperature scale. The onset and end temperature of the melting peak and permeation jumps are marked with dashed lines.

poly(isopropyl acrylate-*co*-A18) copolymers and observed only one packing form along with a very slight increase in *d*-spacing values as the concentration of isopropyl acrylate increased, even though the average side-chain length and amount of crystallinity decreased [2]. They determined that the *d*-spacing values measured for their homopolymers were for the interdigitating packing form. Using the notation from Fig. 8 of part 1 [1], Plate and Shibaev determined that the *d* peak disappeared while the d' peak increased in intensity [1,2,25–27]. They attributed this shift in packing to the distortions in the amorphous backbone caused by the longer side chains crystallizing around the non-crystallizeable comonomers.

We examined the small angle spacings for P(A6-*co*-A22), P(A10-*co*-A14), and P(A10-*co*-A18) copolymer systems in both the crystalline and amorphous states; the spacings are shown in Table 2. Fig. 5(a) shows the *d*-spacings for crystalline polymers and copolymers versus their average side-chain length. The *d*-spacings for the end-to-end packing form, *d* peak, and the interdigitating packing form, d' peak, for *n*-alkyl acrylate homopolymers are shown as the solid and dashed lines, respectively. The solid line for end-to-end packing was taken from Fig. 10 of part 1 [1]. Since the interdigitating, or d' peaks were often too weak to measure, Plate's data were used to compute the dashed line; this has a slope of 1.2 which is approximately half the slope of the line for the end-to-end form [2]. This correlates well with the simple model derived in part 1, where the end-to-end packing formation had a slope of 2 [1,25], and an interdigitating packing formation would be expected to have half that slope. In Fig. 5(a), the crystallizeable/crystallizeable copolymers from Fig. 11(a) of part 1 are represented by the solid square data points in Fig. 5(a) while the P(A6-*co*-A22), P(A10-*co*-A14), and P(A10-*co*-A18) *d*-spacing values are the open data points [1]. In general, most of the *d*-spacing values for our copolymers lie slightly below those for the homopolymers packed end-to-end. This is logical since copolymers form slightly smaller and less perfect crystals than homopolymers. It also shows that, in general, both types of copolymers are predominantly end-to-end packed and their *d*-spacing values increase with the average side-chain length, or crystallinity, of the copolymer. P(A6-*co*-A22) with the composition 75:25 mol% has a larger *d*-spacing value than the homopolymers while P(A10-*co*-A14) with 75:25 mol% and P(A10-*co*-A18) with 75:25 and 50:50 mol% copolymers are closer to the interdigitating

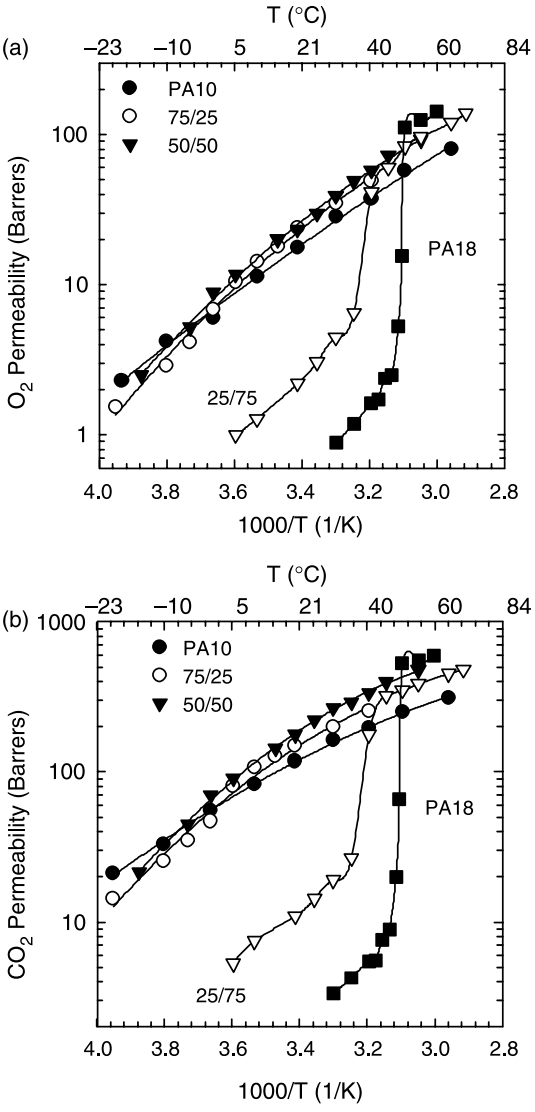

Fig. 10. Permeability of O_2 (a) and CO_2 (b) in P(A10-*co*-A18) copolymers as a function of temperature on Arrhenius coordinates.

packing line. This scatter in the data at lower average side-chain lengths may be similar to the observations by Hsieh and Plate for their copolymers in this local region; however, when considering the broader range of average side-chain lengths, these points are contrary to the majority of the *d*-spacing values observed [2,5,6].

SAXS experiments were also performed on the three sets of copolymers in the amorphous state with the results shown in Fig. 5(b). Homopolymer *d*-spacing values from Fig. 10 of part 1 are plotted as the solid line while copolymers composed of two crystallizeable comonomers from Fig. 11(b) are plotted as the solid square data points [1]. The *d*-spacings for the P(A6-*co*-A22), P(A10-*co*-A14), and P(A10-*co*-A18) copolymers are plotted as the open data points in this figure. As suggested by the model proposed for amorphous copolymers in part 1 of this series [1], the *d*-spacing values of these amorphous copolymers increase with the volume or mass of carbons in the copolymers. Interestingly, the *d*-spacings for the P(A6-*co*-A22) copolymers lies somewhat above the experimental line in the amorphous state ($T > T_m$) while the crystalline *d*-spacings ($T < T_m$) lie below the expected line.

5. Permeation behavior

Figs. 6–11 show the permeability of O_2 and CO_2 through copolymers of P(A6-*co*-A22), P(A10-*co*-A14), and P(A10-*co*-A18). The permeabilities of the copolymers before and after the melting range are described by the expected Arrhenius-temperature relationships [9–14,20,28]. The copolymers that crystallize show the permeation 'jump' on melting as observed previously.

Fig. 6(a) and (b) shows the permeability for O_2 and CO_2 through copolymers of P(A6-*co*-A22). PA 6 is a purely amorphous polymer and, therefore, exhibits a classic Arrhenius-temperature relationship. As the A22 monomer is copolymerized with A6, the copolymers develop the typical well-defined jump in permeability at the melting temperature. Fig. 7(a) and (b) compares the DSC thermograms for P(A6-*co*-A22) copolymers with 25:75 and 75:25 mol%, respectively, to their gas permeability coefficients. As marked by dashed lines in the figures, the melting onset and end temperatures for the thermograms and permeability jumps are approximately the same; this was also the case for PA 22 and P(A6-*co*-A22) with 50:50 mol%. These figures emphasize the existence of well-defined permeation jumps for all the P(A6-*co*-A22) copolymers, including the 75:25% composition that has a limited melting peak.

The permeability coefficients for O_2 and CO_2 through the P(A10-*co*-A14) copolymers are shown in Fig. 8(a) and (b). PA10 does not have a T_m in the experimental temperature range and is, therefore, considered amorphous like PA6. As the concentration of A10 increases in the copolymers, the permeation jumps increase in breadth and decrease in height until they eventually take on the Arrhenius-temperature relationship. Unlike the P(A6-*co*-A22) copolymers and copolymers from part 1 [1] of this series, only two compositions, PA14 and P(A10-*co*-A14) with 25:75%, appear to have strong and well-defined permeation jumps in Fig. 8 [1]. The permeability of O_2 gas through the P(A10-*co*-A14) 25:75, 50:50, and 75:25% compositions is more closely examined in Fig. 9. Fig. 9(a) is similar to Fig. 7(a) for P(A6-*co*-A22) 25:75%; the melting onset and end temperatures for the permeation jumps and DSC thermograms correlate well with each other. The permeation jump is well defined and easily contrasted from the pre- and post-T_m permeability behavior. Fig. 9(b) compares the O_2 permeability response and the DSC endotherm for the P(A10-*co*-A14) 50:50% composition; it is clear that a permeability jump is present and that the melt onset and end temperatures align, although they are not as well defined as for the 25:75% composition in Fig. 9(a). The P(A10-*co*-A14) 75:25% copolymer appears to have no measurable

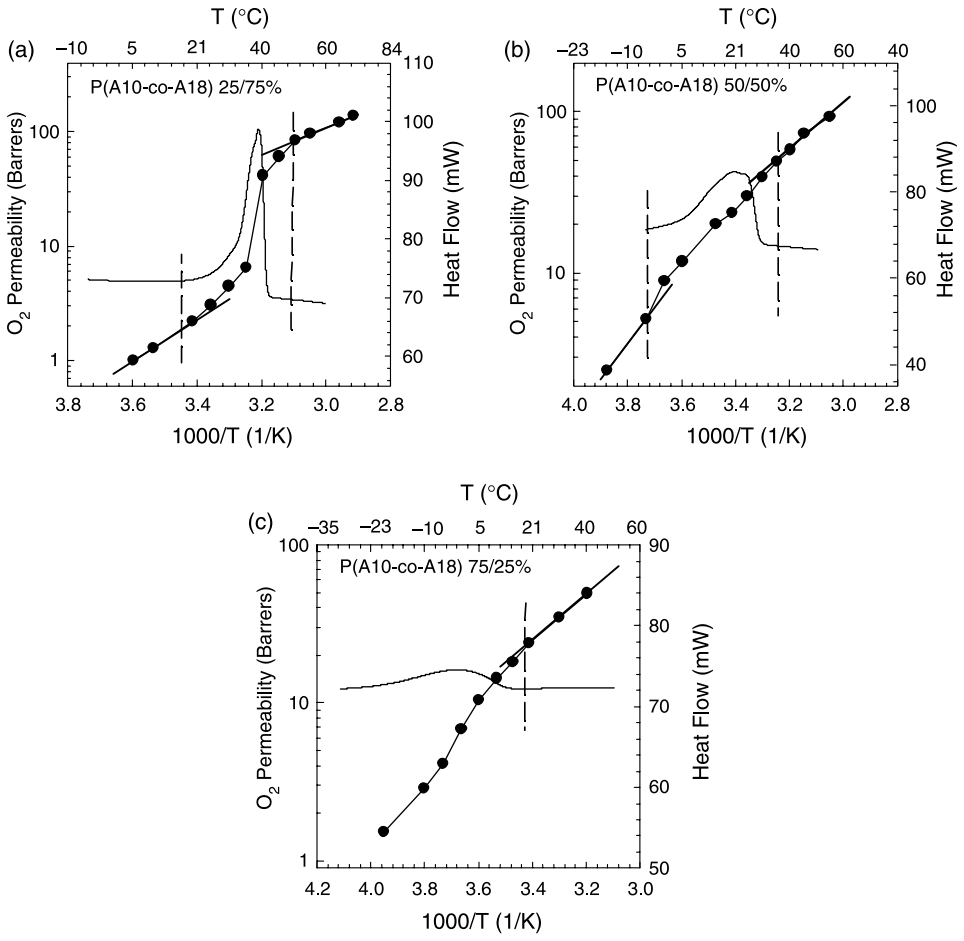

Fig. 11. Permeability in O_2 gas in (a) P(A10-*co*-A18) with 25:75%, (b) 50:50%, and (c) 75:25% as a function of temperature on Arrhenius coordinates with DSC thermograms superimposed on the same temperature scale. The onset and end temperature of the melting peak and permeation jumps are marked with dashed lines.

permeability jump when compared to the other copolymers in Fig. 8; however, when examined in detail as in Fig. 9(c), a slight change in slope of the permeability is present at the onset and end of the melting curve. The melting peak for the copolymer is in the lowest measurable temperature range for both experiments and only the end melting temperature can be accurately assessed; however, it is presumed that the permeation data would show a similar subtle change in slope at the onset temperature for melting.

Permeation data for O_2 and CO_2 are shown in Fig. 10 for copolymers of P(A10-*co*-A18); like the P(A10-*co*-A14) system in Fig. 8, only the PA18 and P(A10-*co*-A18) 25:75% compositions show significant, well-defined permeation jumps. Fig. 11(a) through (c) evaluate the permeation jumps more closely for comparisons with their melting endotherms. P(A10-*co*-A18) with 25:75%, see Fig. 11(a), shows the typical well-defined permeation jump; the melting onset and end temperatures of the endotherm match those of the permeation jump. The 50:50 and 75:25% compositions, Fig. 11(b) and (c), have much less defined permeation jumps; however, like P(A10-*co*-A14) 75:25%, subtle, broad jumps do exist and correlate with the DSC endotherms. This broadening of the permeation jump in these copolymers may ultimately be a solution to modified atmospheric packaging needs by providing a broad, rapid change in permeability with temperature [1].

The onset and end temperatures as defined above are plotted in Figs. 12(a), 13(a), and 14(a) for P(A6-*co*-A22), P(A10-*co*-A14), and P(A10-*co*-A18) copolymer systems, respectively. As expected, linear relationships exist between the onset and end temperatures obtained from the DSC thermograms and from the permeation jump. The onset and end temperature for the permeation jumps are plotted versus the average side-chain length of the copolymers, $\langle n \rangle$, in Figs. 12(b), 13(b), and 14(b) as open and closed data points, respectively. Similar data for P(A14-*co*-A18), taken from Fig. 20(b) of part 1 [1], are superimposed onto the plots as dashed lines to compare the copolymers from part 1 of this series to the systems described here. The P(A6-*co*-A22) system is very different from P(A14-*co*-A18) while the data for P(A10-*co*-A14) and P(A10-*co*-A18) copolymers, see Figs. 13(b) and 14(b), align well with the corresponding results for the P(A14-*co*-A18) system.

Mogri and Paul interpreted the permeability jump behavior of *n*-alkyl acrylates in terms of the modified two-phased model described by Michaels and Bixler for

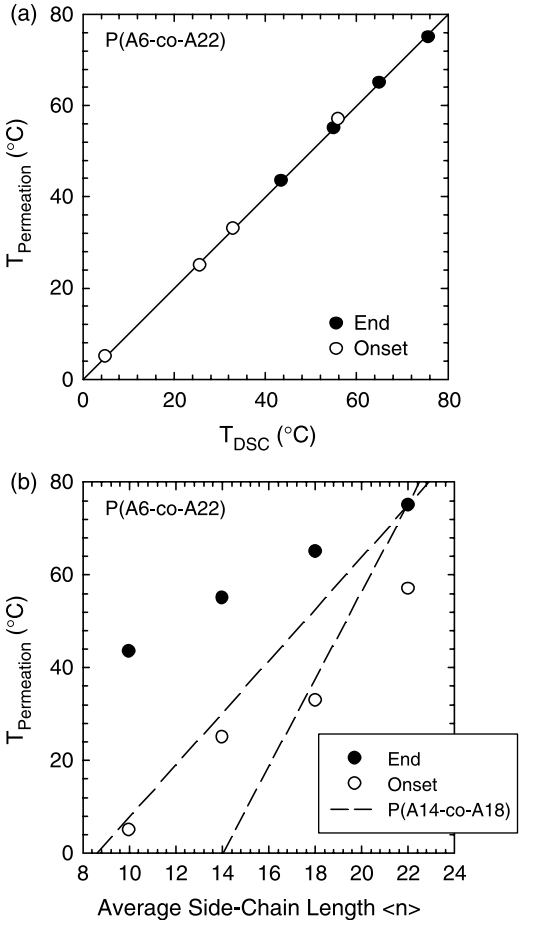

Fig. 12. Relationship between onset and end temperatures for melting of P(A6-*co*-A22) copolymers as measured by permeability jumps and DSC endotherms (a). Correlation between the onset and end temperatures for copolymers of P(A6-*co*-A22) (points) and P(A14-*co*-A18) (dashed-lines) with the average side-chain length (b).

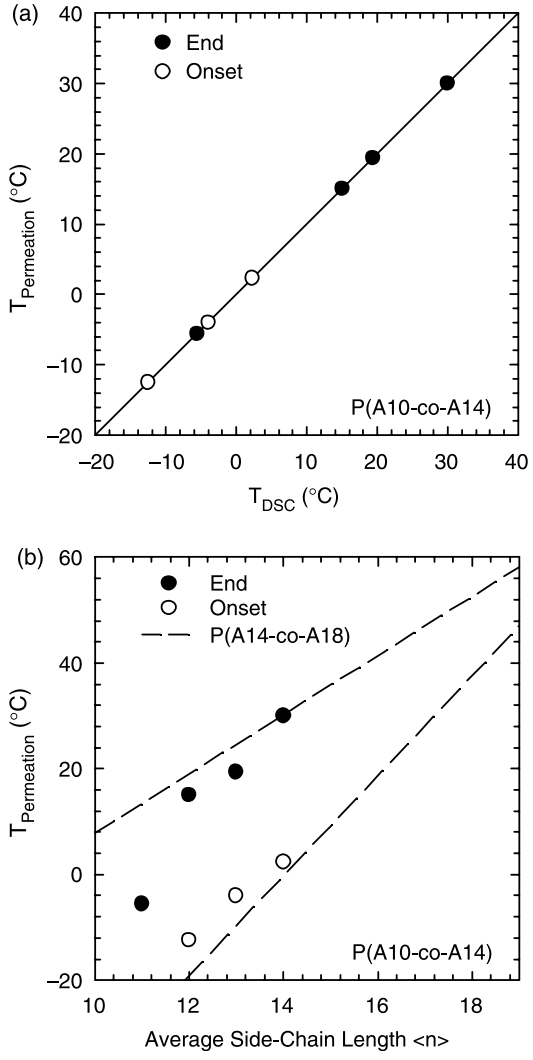

Fig. 13. Relationship between onset and end temperatures for melting of P(A10-*co*-A14) copolymers as measured by permeability jumps and DSC endotherms (a). Correlation between the onset and end temperatures for copolymers of P(A10-*co*-A14) (points) and P(A14-*co*-A18) (dashed-lines) with the average side-chain length (b).

permeation of gases in the semi-crystalline polymers where it is assumed that crystallites are impermeable and all gas transport occurs through the amorphous regions of the polymer [9,10,12,13,29–31]. In these terms, the permeation jump, referenced to a temperature of 35 °C, can be written as

$$\frac{P_c}{P_a} = \frac{P_{35}^{+}}{P_{35}^{-}} = \frac{(1-\phi)}{\tau\beta} \tag{2}$$

where ϕ is the volume fraction of the crystal phase, τ is a tortuosity factor and β accounts for the reduced mobility of the amorphous chain segments by the presence of the crystals.

The magnitudes of the permeation jumps for each copolymer system were calculated using Eq. (2) and are listed in Table 3. Permeation jump ratios for each of the copolymers are plotted versus the penetrant gas diameter in Figs. 15–17. The Arrhenius activation energies in the semi-crystalline state (E_c) are greater than those in the amorphous phases (E_a); therefore, the reference temperature to which the permeability data are extrapolated affects the jump ratio calculations [9,10,13]. Hence, we use a median temperature for all the copolymers in a system as the reference temperature: 35 °C for P(A6-*co*-A22) and P(A10-*co*-A18), and 10 °C for P(A10-*co*-A14). Using a 35 °C reference temperature for P(A10-*co*-A14) results in slightly skewed jump ratios because the melting temperatures of the copolymers in this system as significantly lower than 35 °C. Although the onset and end melting temperatures could be observed for most of the copolymers in Figs. 9 and 11, the permeability-temperature relationship could not always be measured adequately well enough below T_m to draw a conclusive Arrhenius-temperature line. Therefore, permeability jump ratios were not calculated for all the compositions.

Figs. 15–17 show that the jump ratios for all the copolymer systems increase with increasing average

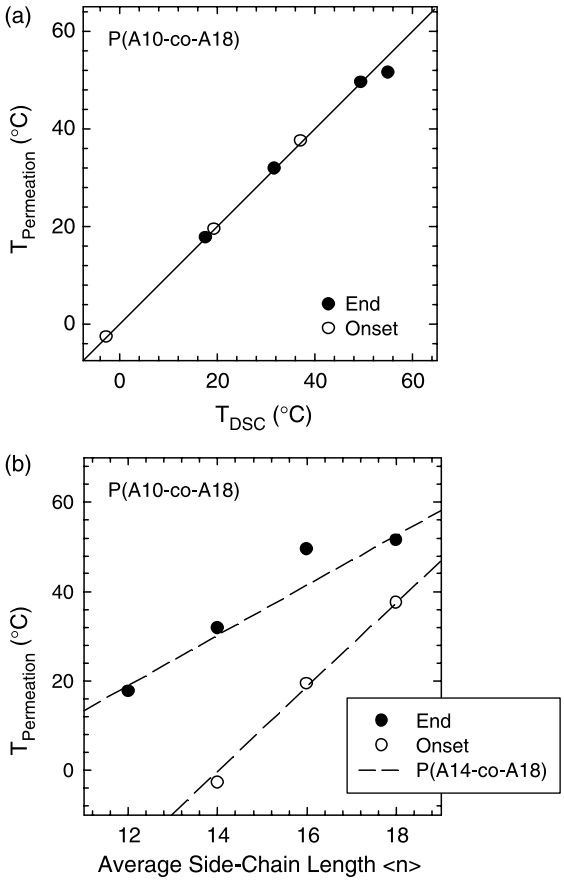

Fig. 14. Relationship between onset and end temperatures for melting of P(A10-*co*-A18) copolymers as measured by permeability jumps and DSC endotherms (a). Correlation between the onset and end temperatures for copolymers of P(A10-*co*-A18) (points) and P(A14-*co*-A18) (dashed-lines) with the average side-chain length (b).

side-chain length as well as penetrant diameter. The results are similar to those for the homopolymers (Fig. 14) and copolymer systems (Fig. 21) reported in part 1 [1]. As explained in part 1, the permeation jump is partially the result of melting the impermeable crystallites thus eliminating the tortuous path for the molecules as well as the effects included in the chain immobilization factor, β [1,9,13]. For each of the copolymer systems, an increase in the average side-chain length increases the crystallinity and the change in tortuosity upon melting. The increase in jump ratios with penetrant gas diameter may be attributed to the chain immobilization factor, β, which accounts for how the segmental dynamics of the polymer are affected by the crystallites. This factor becomes greater the larger the penetrant gas molecule. The permeation jump ratios for the copolymers are also plotted versus the average side-chain length and compared to those for the homopolymers from Fig. 15 of part 1 in Figs. 18–20 [1]. The crystallinity of the copolymers and homopolymers increases with side-chain length which correlates with the increasing jump ratios. Both crystalline/crystalline and crystalline/non-crystalline copolymers are less crystalline than homopolymers; reflected in the smaller jump ratios compared to the homopolymers in Figs. 21 and 22 of part 1 [1] and Fig. 18 shown here; other similar comparisons are available, elsewhere [24] (Fig. 18).

The direct relationship between heat of fusion and permeability jump ratios for these copolymers and homopolymers is illustrated in Fig. 19 for O_2; similar relationships hold for all other gases. The jump ratios for homopolymers (open circles) and both crystallizeable/crystallizeable and crystallizeable/non-crystallizeable copolymers (closed circles) increase with increasing heat of fusion. This illustrates the usefulness of simple DSC analysis for predicting the jumps in gas permeabilities for these copolymers.

6. Conclusions

Poly(*n*-alkyl acrylate) copolymer systems containing a crystallizeable comonomer and a non-crystallizeable or slightly crystallizeable comonomer were studied with respect to their thermal behavior, SAXS structure, and gas permeability properties. These copolymer systems were compared to copolymers with two crystallizeable comonomers. The non-crystallizeable comonomers affect the copolymer by interrupting and impeding the crystallizeable side chains from forming perfect crystals. The formation of smaller and less perfect crystals causes a 'depression' in the melting temperature. Unlike copolymers with two crystallizeable comonomers that enter the lattice and alter the basic nature of the crystal, non-crystallizeable comonomers only impede crystal formation; therefore, the co-crystallizing side chains can affect the T_m more than the latter.

PA 10 is an unusual polymer in that its side chains are on the border of being crystallizeable; therefore, the thermal properties of several copolymers containing A10 were evaluated and compared to other copolymers. It was determined that the T_m and ΔH_f for copolymers of P(A6-*co*-A22) and P(A8-*co*-A22) exhibit melting point depression caused by the non-crystallizeable side chains limiting crystal formation, while the A10 in P(A10-*co*-A22) behaved like a crystallizeable comonomer which enters the lattice and alters the nature of the crystal.

Limited small angle X-ray scattering (SAXS) experiments were used to measure the crystalline and amorphous *d*-spacings for three different copolymer systems. It was determined that the crystalline side chains of the P(A6-*co*-A22), P(A10-*co*-A14), and P(A10-*co*-A18) copolymers have a predominantly end-to-end packing form with slightly smaller *d*-spacing values attributed to the formation of smaller and less perfect crystals. As was expected, the amorphous copolymers have *d*-spacings similar to those of the homopolymers and copolymers examined in part 1 [1].

The gas permeability behavior of these copolymer systems were determined and compared to the systems described in part 1 [1]. Like the crystallizeable-crystallizeable copolymers, the P(A6-*co*-A22) copolymers followed the temperature trends measured by DSC. The jump ratios and breadths

Table 3
Activation energy and permeability data extrapolated to 10 and 35 °C for various gases through poly(*n*-alkyl acrylate) copolymers

Copolymer	Monomer 1 (mol%)		Gas					
			He	H_2	O_2	N_2	CH_4	CO_2
P(A6-*co*-A22)	75	E_a	2.7	2.9	3.7	1.7	3.5	1.6
		E_c	6.1	9.3	10.5	12.3	12.6	4.8
		P^+_{35}	106.6	154.3	57.1	33.0	63.7	301.7
		P^-_{35}	13.9	13.9	2.4	0.7	1.7	12.9
		P^+_{35}/P^-_{35}	7.7	11.1	23.4	44.9	37.2	23.4
P(A6-*co*-A22)	50	E_a	2.9	2.9	6.2	2.3	3.9	3.1
		E_c	6.0	6.0	6.2	7.9	9.8	5.9
		P^+_{35}	110.1	162.9	25.4	24.3	32.5	224.0
		P^-_{35}	15.2	17.2	3.0	1.1	2.2	15.0
		P^+_{35}/P^-_{35}	7.3	9.5	8.5	22.6	15.1	15.0
P(A6-*co*-A22)	25	E_a	5.7	3.1	5.1	5.7	5.5	2.4
		E_c	7.6	7.1	5.5	9.2	7.3	5.8
		P^+_{35}	87.1	184.0	32.1	11.5	29.9	186.3
		P^-_{35}	45.1	55.5	8.0	4.9	11.6	72.5
		P^+_{35}/P^-_{35}	1.9	3.3	4.0	2.4	2.6	2.6
P(A10-*co*-A14)	75	E_a	3.5	2.2	4.2	4.9	5.8	3.1
		E_c	–	–	–	–	–	–
		P^+_{10}	35.1	63.3	26.9	8.5	12.8	136.5
		P^-_{10}	–	–	–	–	–	–
		P^+_{10}/P^-_{10}	–	–	–	–	–	–
P(A10-*co*-A14)	50	E_a	6.6	4.4	7.9	8.1	8.6	5.4
		E_c	–	–	–	–	–	–
		P^+_{10}	21.8	36.2	19.2	6.1	14.6	139.3
		P^-_{10}	–	–	–	–	–	–
		P^+_{10}/P^-_{10}	–	–	–	–	–	–
P(A10-*co*-A14)	25	E_a	5.1	3.6	4.8	7.9	8.3	2.7
		E_c	4.4	3.0	6.5	6.5	4.8	5.1
		P^+_{10}	28.0	54.3	33.5	6.9	17.2	209.0
		P^-_{10}	9.7	9.5	4.6	0.9	1.3	21.5
		P^+_{10}/P^-_{10}	2.9	5.7	7.4	7.8	13.1	9.7
P(A10-*co*-A14)	0	E_a	5.8	5.7	5.7	6.5	6.5	3.7
		E_c	6.1	6.4	8.7	10.1	8.6	6.6
		P^+_{10}	22.70	42.30	24.80	8.70	25.80	177.50
		P^-_{10}	5.00	5.90	1.90	0.51	1.30	8.30
		P^+_{10}/P^-_{10}	4.50	7.10	13.20	17.30	20.10	21.50
P(A10-*co*-A18)	75	E_a	8.3	8.1	6.6	9.4	6.6	4.9
		E_c	–	–	–	–	–	–
		P^+_{35}	46.5	45.7	41.4	48.8	41.5	225.0
		P^-_{35}	–	–	–	–	–	–
		P^+_{35}/P^-_{35}	–	–	–	–	–	–
P(A10-*co*-A18)	50	E_a	7.6	8.2	6.4	9.0	10.4	7.3
		E_c	–	–	–	–	–	–
		P^+_{35}	56.8	98.6	49.6	21.2	58.3	291.1
		P^-_{35}	–	–	–	–	–	–
		P^+_{35}/P^-_{35}	–	–	–	–	–	–
P(A10-*co*-A18)	25	E_a	6.4	6.1	5.4	6.5	6.0	3.4
		E_c	7.3	8.5	9.4	11.5	10.6	7.8
		P^+_{35}	78.1	137.3	55.4	17.7	42.4	272.0
		P^-_{35}	18.7	23.1	4.9	1.6	3.6	21.6
		P^+_{35}/P^-_{35}	4.2	6.0	11.3	11.0	11.7	12.6

Note that monomer 1 refers to the first monomer listed in the copolymer, i.e. for P(A14-*co*-A18), monomer 1 refers to A14. The activation energies E_a and E_c have units of kcal/mol while the permeability coefficients P^+_{35}, P^-_{35}, P^+_{10}, and P^-_{10} have units of Barrers, i.e. 10^{-10} cm^2(STP) cm/(cm^2 cm Hg s).

correlate well with the DSC thermograms. The permeation jumps for the P(A10-*co*-A14) and P(A10-*co*-A18) copolymer systems, however, are much smaller and less defined with increasing A10 concentration. While the onset and end melting temperatures and permeation jump temperatures aligned well, as observed with other systems, the onset and end of the permeation jump were very subtle due to its broadening.

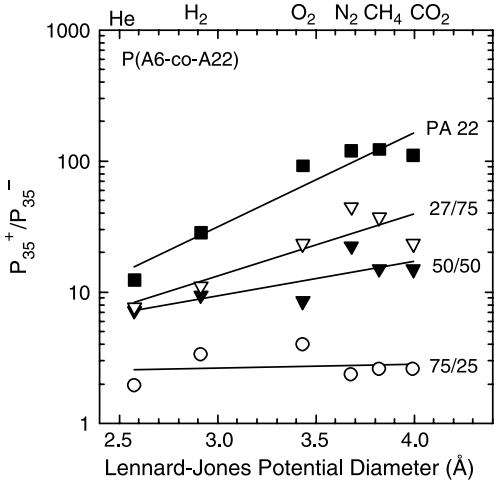

Fig. 15. Permeation jump ratios calculated at 35 °C for P(A6-*co*-A22) copolymers shown as a function of the penetrant molecule diameter.

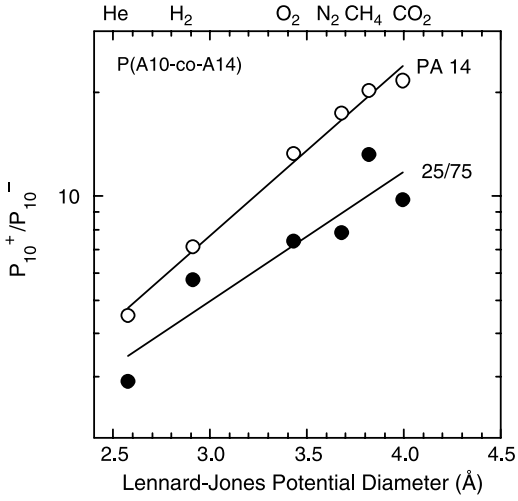

Fig. 16. Permeation jump ratios calculated at 10 °C for P(A10-*co*-A14) copolymers shown as a function of the penetrant molecule diameter.

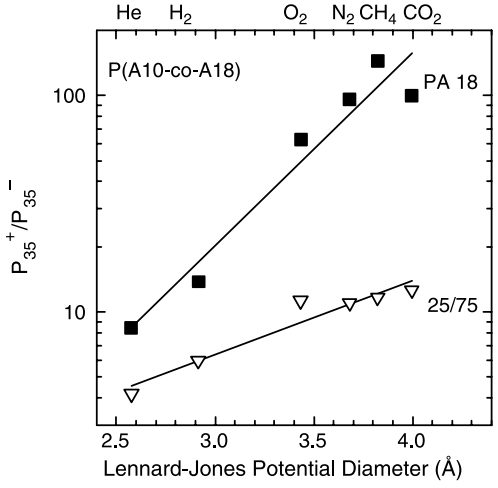

Fig. 17. Permeation jump ratios calculated at 35 °C for P(A10-*co*-A18) copolymers shown as a function of the penetrant molecule diameter.

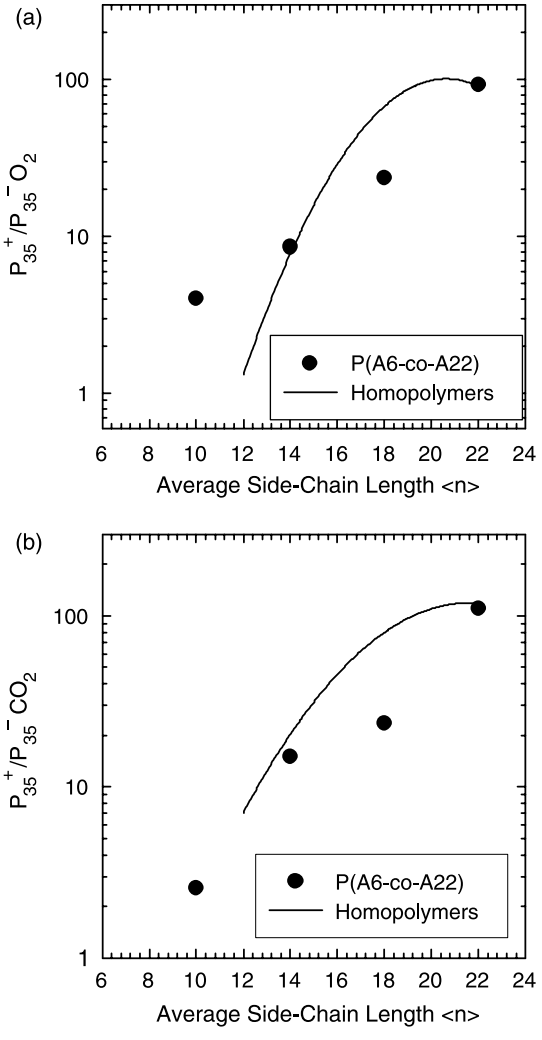

Fig. 18. Permeation jump ratios calculated at 35 °C for P(A6-*co*-A22) copolymers and homopolymers shown as a function of the average side-chain length ⟨*n*⟩.

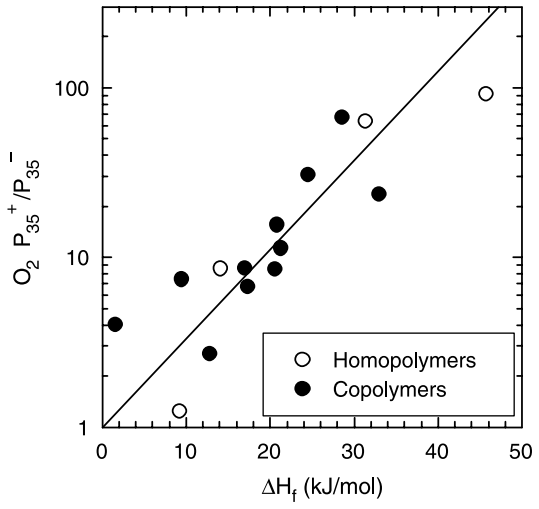

Fig. 19. Relationship between permeation jump ratios and heats of fusion for *n*-alkyl acrylate homopolymers (open points) and copolymers (closed points).

Acknowledgements

This research was funded by National Science Foundation Grant number CTS-0086961 administered by the Division of Chemical and Transport Systems-Separation and Purification Processes Program.

References

[1] O'Leary KA, Paul DR. Polymer. 2006 in press, doi: 10.1016/j.polymer.2005.12.005.
[2] Plate NA, Shibaev VP. Comb-shaped polymers and liquid crystals. New York: Plenum Press; 1987 p. 1–104.
[3] Rehberg CE, Fisher CH. J Am Chem Soc 1944;66:1203.
[4] Greenberg SA, Alfrey T. J Am Chem Soc 1954;76:6280.
[5] Hsieh HWS. PhD Thesis. Polytechnic Institute, New York; 1976.
[6] Hsieh HWS, Post B, Morawetz H. J Polym Sci, Polym Phys 1976;14(7):1241.
[7] Jordan Jr EF, Feldeisen DW, Wrigley AN. J Polym Sci, Polym: Chem Ed 1971;9(11):3349.
[8] Jordan Jr EF, Feldeisen DW, Wrigley AN. J Polym Sci, Polym: Chem Ed 1971;9(7):1835.
[9] Mogri Z. PhD Thesis. University of Texas, Austin; 2001.
[10] Mogri Z, Paul DR. Polymer 2000;42(6):2531–42.
[11] Mogri Z, Paul DR. J Membr Sci 2000;175(2):253.
[12] Mogri Z, Paul DR. Polymer 2001;42(18):7781.
[13] Mogri Z, Paul DR. Polymer 2001;42(18):7765.
[14] O'Leary K, Paul DR. Polymer 2004;45(19):6575.
[15] Kirkland BS, Paul DR. Unpublished results.
[16] Stewart RF. US Patent No. 87-120399, Landec Labs., Inc., USA; 1989.
[17] Clark R, Stewart R, Yoon V, Schultz D, McClary B. US Patent No. 453018, Landec Corporation, USA; 2002.
[18] Hirabayashi T, Yokota K. Polym J 1988;20(8):693.
[19] Hirabayashi T, Yokota K. Polym J 1987;19(9):1115.
[20] Paul DR, Clarke R. J Membr Sci 2002;208(1-2):269.
[21] Paul DR, Mogri Z. ACS Natl Meet; March 2000, IEC-130.
[22] Clark R, Stewart R, Yoon V, Schultz D, McClary B. US Patent No. 96-US7939, Landec Corporation, USA; 1996.
[23] Greene L, Phan L, Schmitt E, Mohr J. ACS Symp Ser 1993;520:244.
[24] O'Leary KA. PhD Dissertation. University of Texas, Austin; 2005.
[25] Chu B, Hsiao BS. Chem Rev 2001;101(6):1727.
[26] Fairclough JPA, Hamley IW, Terrill NJ. Radiat Phys Chem 1999;56(1-2):159.
[27] Hadjichristidis N, Pispas S, Floudas G. Block copolymers. 1st ed. Hoboken: Wiley; 2003 p. 347.
[28] Mogri Z, Paul DR. J Polym Sci, Part B 2001;39(10):979.
[29] Michaels AS, Bixler HJ. J Polym Sci 1961;50:413.
[30] Michaels AS, Bixler HJ. J Polym Sci 1959;41:53.
[31] Michaels AS, Bixler HJ. J Polym Sci 1961;50:393.